NASA TECHNICAL NOTE

NASA TN D-5969

NASA TN D-5969

APOLLO ABLATOR THERMAL PERFORMANCE AT SUPERORBITAL ENTRY VELOCITIES

by Donald M. Curry and Emily W. Stephens

Manned Spacecraft Center
Houston, Texas 77058

NATIONAL AERONAUTICS AND SPACE ADMINISTRATION • WASHINGTON, D. C. • SEPTEMBER 1970

1. REPORT NO.
NASA TN D-5969

2. GOVERNMENT ACCESSION NO.

3. RECIPIENT'S

4. TITLE AND SUBTITLE

APOLLO ABLATOR THERMAL PERFORMANCE AT SUPERORBITAL ENTRY VELOCITIES

5. REPORT DATE
September 1970

6. PERFORMING ORGANIZATION CODE

7. AUTHOR(S)
Donald M. Curry and Emily W. Stephens, MSC

8. PERFORMING ORGANIZATION REPORT NO.
MSC S-247

9. PERFORMING ORGANIZATION NAME AND ADDRESS
Manned Spacecraft Center
Houston, Texas 77058

10. WORK UNIT NO.
914-11-20-11-72

11. CONTRACT OR GRANT NO.

12. SPONSORING AGENCY NAME AND ADDRESS
National Aeronautics and Space Administration
Washington, D.C. 20546

13. REPORT TYPE AND PERIOD COVERED
Technical Note

14. SPONSORING AGENCY CODE

15. SUPPLEMENTARY NOTES

16. ABSTRACT

Objectives of the Apollo 4 and 6 missions included the demonstration of the capability of the ablative heat shield to survive entry at lunar-return velocities and the collection of data necessary to support the analytical qualification of the ablative heat shield for manned lunar-return missions. Results of ground test programs, as well as the Apollo 4 and 6 flight tests, are discussed in relation to the verification of the analytical ablation model. Ablator cores taken from the Apollo command module were evaluated to obtain the thermophysical property values used in the analytical model. Temperatures were measured by thermocouples located in depth in the ablator. Char-thickness measurements were obtained from char sensors in the heat shield and from ablator cores. The results of the thermal performance evaluation and comparisons of measured and predicted data have been used to establish a confidence level in the analytical model used to make preflight predictions and will provide the information necessary to improve prediction techniques.

17. KEY WORDS (SUPPLIED BY AUTHOR)
* Charring Ablator
* Thermal Performance
* Apollo Heat Shield

18. DISTRIBUTION STATEMENT
Unclassified - Unlimited

19. SECURITY CLASSIFICATION (THIS REPORT)
None

20. SECURITY CLASSIFICATION (THIS PAGE)
None

21. NO. OF PAGES
28

22. PRICE*
$3.00

*For sale by the Clearinghouse for Federal Scientific and Technical Information
Springfield, Virginia 22151

APOLLO ABLATOR THERMAL PERFORMANCE AT SUPERORBITAL ENTRY VELOCITIES

By Donald M. Curry and Emily W. Stephens
Manned Spacecraft Center

SUMMARY

The Apollo command module heat shield has been successfully flight tested at both earth-orbital and lunar-return entry speeds. The flight tests demonstrated the thermal performance of the ablative heat shield and provided data necessary for thermal performance analyses in which an analytical model was used. Analysis of the flight test data substantiated the validity of the analytical techniques used for design and operational qualification of the Apollo ablative heat shield. Comparisons of measured and postflight-predicted thermal performance data for the Apollo 4 and 6 heat shields were used (1) to establish a confidence level in the analytical model developed to make preflight predictions of ablator performance and (2) to yield insights useful in the improvement of prediction techniques.

INTRODUCTION

During a lunar-return entry, the Apollo command module (CM) experiences a rapid rise in convective- and radiative-heating rates associated with atmospheric braking. Hence, prior to manned missions, an analytical procedure was required for qualifying the CM ablative heat shield for a lunar-return entry. Thus, four unmanned Apollo missions had as their prime objectives (1) the demonstration of the capability of the ablative heat shield to survive entry and (2) the collection of data necessary to verify the techniques used in the analytical qualification of the ablative heat shield. These four unmanned missions were Apollo 1 and 3, in which the CM entered the atmosphere from earth orbit, and Apollo 4 and 6, in which the CM entered the atmosphere at superorbital entry velocities.

Although the unmanned flight tests provided a demonstration of the adequacy of the ablative heat shield, an analytical qualification was required to afford a detailed thermal performance analysis of the Apollo heat-shield ablator for spacecraft entries at design conditions (ref. 1), as well as throughout the operational entry-corridor conditions (ref. 2). The same analytical model was used to qualify the ablative heat shield for both design and operational conditions.

Although results from test programs performed in ground facilities were used in the initial formulation of the analytical ablator model (refs. 1 and 3), thermal data

obtained from the unmanned flight tests were used to refine the analytical model for prediction of flight performance. The thermophysical property values used in the analytical model were obtained from laboratory-charred test specimens (ref. 4), and the accuracy of these values was substantiated by measurements made on ablator cores taken from flight-tested spacecraft. Temperatures measured during the flight tests by thermocouples located in depth in the ablator and char thicknesses measured from ablator cores and by char sensors in the ablator were compared with analytically predicted ablator response to establish the accuracy of the analytical methods used in making the predictions.

The purpose of this report is to present the verification of the analysis by showing comparisons between the analytical predictions of heat-shield performance and the data obtained from the unmanned flight tests. Particular emphasis is placed on the data obtained from Apollo 4, the mission that most closely simulated a lunar-return entry.

SYMBOLS

A_1	Arrhenius coefficient (eq. (4)), hr^{-1}
A_2	constant used in the coking relation (eq. (8)), hr^{-1}
a	specie weighing factor
B	blowing parameter
B_1	Arrhenius coefficient (eq. (4)), $^\circ R$
B_2	constant used in the coking relation (eq. (8)), $^\circ R$
C	constant (eq. (6))
$C_{o,e}$	oxygen concentration at the boundary-layer edge
c_p	specific heat, $Btu/lb_m\text{-}^\circ R$
E	activation energy, $Btu/lb_m\text{-mole}$
F_{conv}	multiplication factor for the convective-heating rate
F_{rad}	multiplication factor for the radiative-heating rate
H	enthalpy, Btu/lb_m

H_v heat of degradation, $Btu/lb_m\text{-}^\circ R$

K thermal conductivity, $Btu/ft\text{-}hr\text{-}^\circ R$

K_o collision frequency, $lb_m/\left(ft^2\text{-}sec\text{-}atm^{\eta_2}\right)$

$\dot{m}$ mass-loss rate, $lb_m/ft^2\text{-}hr$

P_o local pressure, atm

P_o/P_t ratio of local pressure and total pressure

Q_K heat of deposition, Btu/lb_m

$\dot{q}$ heat flux, $Btu/ft^2\text{-}sec$

R universal gas constant, $Btu/lb_m\text{-}mole\text{-}^\circ R$

R_c maximum body radius, in.

Re_{tr} transition Reynolds number for turbulence

ST Stanton number

S/R_c surface-wetted length from the geometric center of the aft heat shield divided by the maximum body radius

$\dot{s}$ surface-recession rate, in/sec

T temperature, $^\circ R$

t time, sec

u velocity, ft/sec

W_x surface-wetted length, measured from the stagnation point, in.

X_c longitudinal location, referenced to the CM (fig. 1), in.

x distance, in.

Y_c, Z_c lateral CM axes (figs. 1 and 4(a)), in.

α	angle of attack, deg
η_1	order of reaction (eq. (4))
η_2	order of reaction (eq. (5))
θ	angular designation associated with the Y_c-Z_c plane (fig. 4(a)), deg
ρ	density, lb_m/ft^3
$\dot{\rho}_{coke}$	rate of density increase caused by deposition, lb_m/ft^3-hr
ψ	convective-heat blocking ratio

Subscripts:

BL	boundary layer
char	char
comb	combustion
conv	convective
diff	diffusion controlled
e	edge
g	gas
HW	hot wall
kine	kinetic controlled
o	nonblowing value
rad	radiative
rr	reradiated
S	surface
subl	sublimation
t	total

v	virgin
WB	with blowing
w	wall

ENTRY HEATING

The range of entry heating conditions that can be experienced by the Apollo CM during a lunar-return entry is discussed in reference 1. The area of highest heating (at the flight angle of attack) of the spacecraft is located on the blunt entry face of the CM pitch plane near the windward meridian of the aft-heat-shield toroidal section (fig. 1). The theoretical convective- and radiative-heating rates near the flight stagnation region for Apollo 4 are shown in figure 2. The analytically determined cold-wall convective-heating rate used as input to the ablator thermal performance computer program was corrected to include the effects of local mass injection.

Data obtained from supersonic wind-tunnel tests were used to define a laminar heating distribution for various angles of attack α over the Apollo CM (ref. 5). A heating distribution for a typical Apollo entry angle of attack is shown in figure 3 as a function of surface-wetted length from the geometric center of the aft heat shield divided by the maximum body radius S/R_c. Heating factors for the flight angle of attack were obtained by interpolation between heating distribution curves shown in reference 5. The local heating rates used in the ablator thermal performance analyses were obtained by use of the interpolated heating distribution curve and the theoretical stagnation heating rate. The heating factors used for the calculations discussed in this paper are presented in table I.

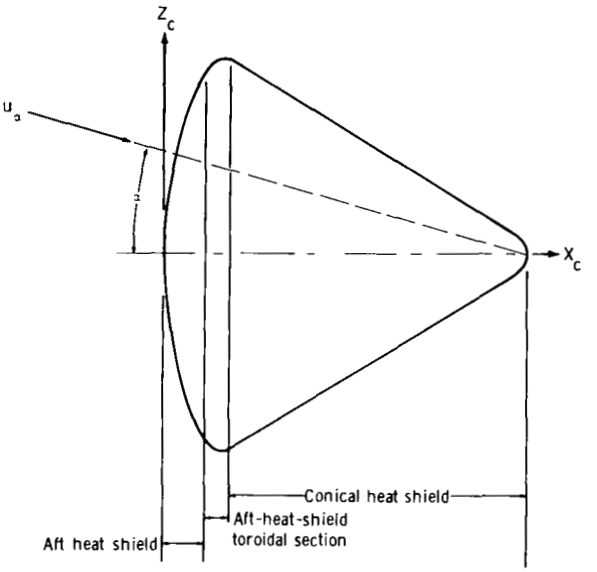

Figure 1. - Apollo CM configuration taken through the pitch plane.

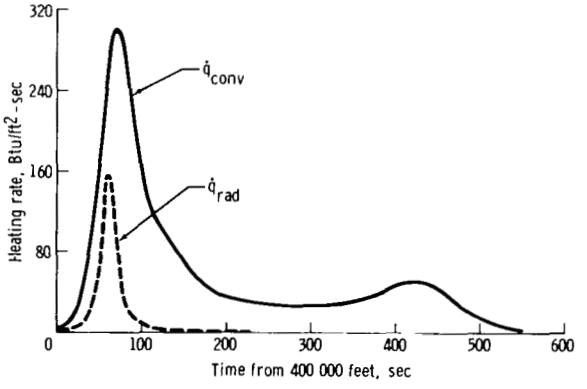

Figure 2. - Theoretical convective- and radiative-heating rates at $S/R_c = 0.9875$ for the Apollo 4 mission.

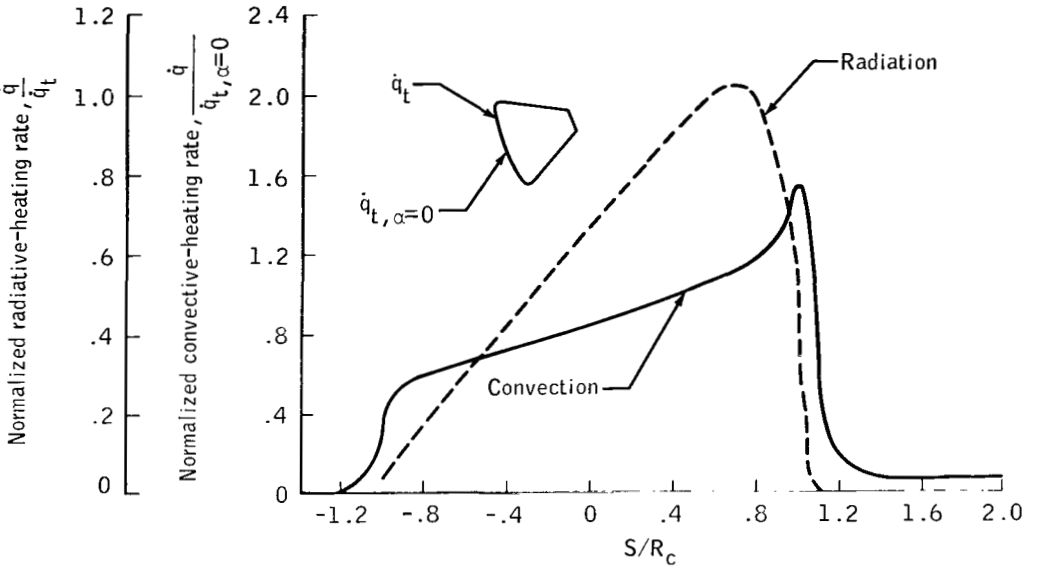

Figure 3. - Apollo CM convective- and radiative-heating-rate distribution for a typical entry angle of attack.

TABLE I. - HEATING CONFIGURATION FACTORS

Mission	Location summary		Heating rate factors		W_x, in.	P_o/P_t	Re_{tr}
			F_{conv}	F_{rad}			
Apollo 4	Y_c = 0 in.	Z_c = 71.8 in.	0.924	1.227	1.31	0.84	80 000
	Y_c = 2 in.	Z_c = -50.0 in.	.400	.463	8.56	.56	80 000
	X_c = 18.2 in.	θ = 182°15'	.181	.075	8.30	.10	80 000
	X_c = 50.0 in.	θ = 93°27'	.056	0	5.13	.03	80 000
	X_c = 78.9 in.	θ = 274°19'	.006	0	17.6	.01	20 000
Apollo 6	Y_c = 0 in.	Z_c = 71.8 in.	.924	1.227	1.31	.84	80 000

HEAT-SHIELD MEASUREMENTS

Thermal performance data for the ablative heat shield were obtained from thermocouples and char sensors. In this paper, the ablative heat shield will be discussed in terms of the aft heat shield, the aft-heat-shield toroidal section (located at the interface between the aft and the conical heat shields), and the conical heat shield. The heat-shield configuration is shown in figure 1. Instrumentation was placed in several locations on each section of the heat shield to facilitate a thermal performance analysis of each section.

Temperatures were measured by thermocouples located in depth in the ablator to determine the ablator temperature profile and by thermocouples located at the bondline, or interface, of the ablator and the stainless steel honeycomb. A detailed discussion of the instrumentation locations, installation techniques, and instrumentation accuracy is presented in reference 6. Chromel-alumel thermocouples were used at locations where the temperature was predicted to be less than 2400° F, except at the bondline, where chromel-constantan thermocouples were used. Tungsten-rhenium thermocouples were used to measure temperatures greater than 2400° F. Figure 4(a) shows the location of the thermocouples on the aft heat shield, and figure 4(b) shows the location of thermocouples on the aft-heat-shield toroidal section and on the conical heat shield. (The compression pads and shear compression pads shown in figures 4(a) and 5 are structural attachment points that penetrate the aft heat shield. Although thermocouples were located in the vicinity of these pads, as shown, only the responses of thermocouples located in smooth body regions are discussed in this paper.)

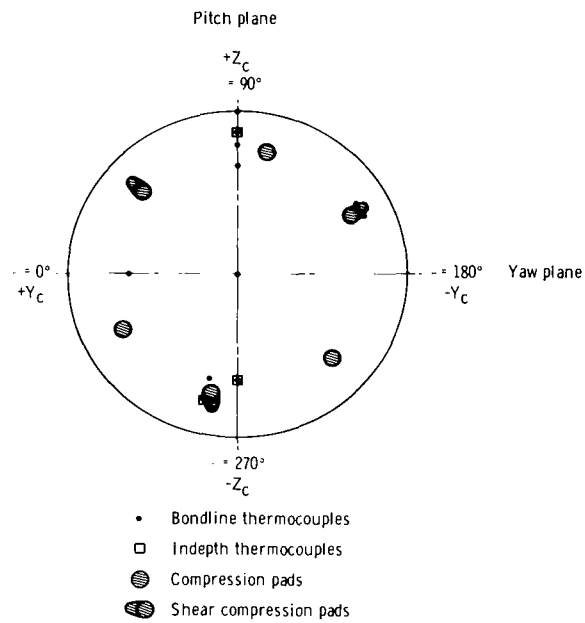

(a) Aft heat shield, forward-looking view.

Figure 4. - Apollo 4 CM, showing thermocouple locations.

Char-thickness measurements were obtained from char sensors located at various depths in the ablator. The char sensors were located adjacent to the stacks of indepth thermocouples located on the aft-heat-shield pitch plane at $Z_c = 71.8$ inches and at $Z_c = -50.0$ inches.

Ablator cores were removed from the recovered heat shields to provide additional measurements for interpretation of the ablator performance. These cores (fig. 5) were cross sectioned to obtain measurements of the surface recession and the char depth. Cross-sectional views of two typical postflight ablator cores are shown in figure 6. From an analysis of such cores,

the effects of the local environment at uninstrumented body locations on the thermal response of the ablator could be determined, and the thermophysical properties used in making performance predictions could be substantiated.

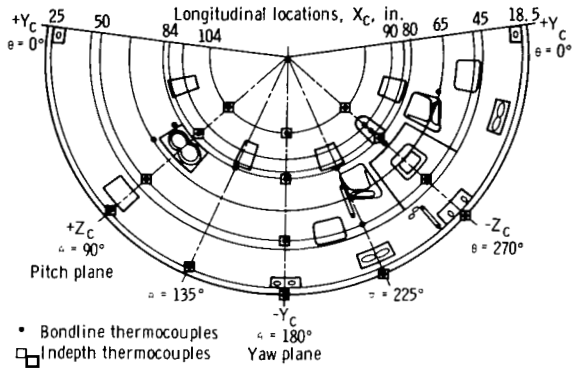

(b) Aft-heat-shield toroidal section and conical heat shield.

Figure 4. - Concluded.

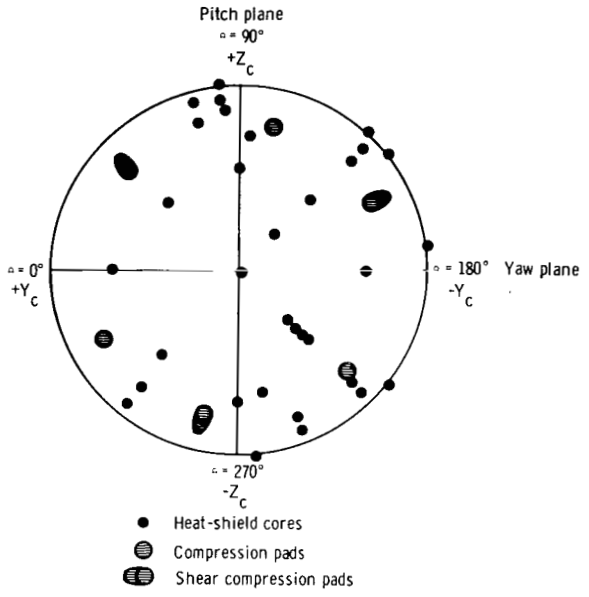

Figure 5. - Apollo 4 aft heat shield, showing locations of ablator cores taken for analysis, forward-looking view.

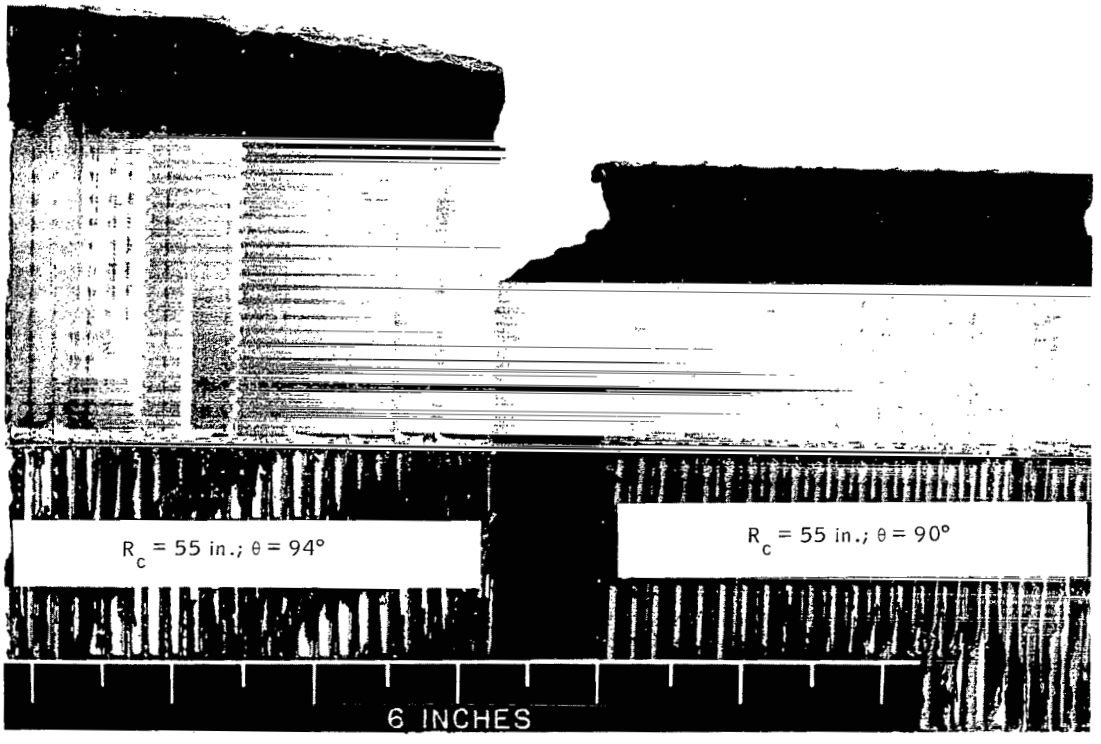

Figure 6. - Cross-sectional view of typical Apollo 4 aft-heat-shield ablator cores.

ABLATION ANALYSIS

The Apollo CM ablator is a low-density phenolic-epoxy novolac material that pyrolyzes as it is heated, yielding a pyrolysis gas and a porous char residue. Preflight and postflight predictions of ablator response to the entry environment were made by using a one-dimensional heat- and mass-transfer computer program designated as STAB II and described in reference 3. This computer program is based on a complex model in which the ablator is assumed to be divided into three distinct zones: the char-layer, reaction, and virgin zones (fig. 7).

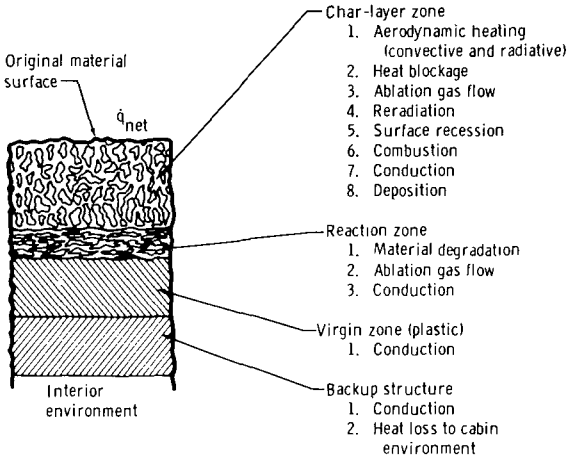

Figure 7. - Schematic diagram of charred heat-shield ablator.

The STAB II computer program predicts the transient temperatures and density histories of an ablation material exposed to a hyperthermal environment (defined in terms of local heating rates and pressure). The computation procedure is an implicit finite-difference solution for one ablating material and several backup materials. A discussion of the assumptions, approximations, and capabilities of the STAB II computer program is presented in reference 3.

Extensive tests of ablator samples in simulated entry environments were performed to verify the adequacy of the analytical model used for preflight prediction of ablator thermal performance. A comparison of these ground test results with the analytical predictions is presented in reference 1.

As a result of the experimental investigations discussed in reference 4, the energy equation presented in reference 3 has been modified to include an energy source term.

$$\rho c_p \frac{\partial T}{\partial t} = \frac{\partial}{\partial x}\left(K \frac{\partial T}{\partial x}\right) + \dot{m}_g c_{p,g} \frac{\partial T}{\partial x} + H_v \frac{\partial \rho}{\partial t} + Q_K(x) \qquad (1)$$

where $\rho c_p \frac{\partial T}{\partial t}$ = rate of energy stored

$\frac{\partial}{\partial x}\left(K \frac{\partial T}{\partial x}\right)$ = heat conducted

$\dot{m}_g c_{p,g} \frac{\partial T}{\partial x}$ = heat convected by pyrolysis gases

$H_v \frac{\partial \rho}{\partial t}$ = local rate of heat absorption caused by primary decomposition of the virgin plastics

$Q_K(x)$ = energy source term (this term was added to the energy equation and represents the additional modes of heat absorption, or liberation, such as the coking phenomenon)

The boundary condition at the outer surface of the material (ref. 1) can be written as

$$\psi \dot{q}_{HW,o} + \dot{q}_{rad} + \dot{q}_{comb} - \dot{q}_{rr} - \dot{q}_{subl} = -K \frac{\partial T}{\partial x} \tag{2}$$

where $\psi \dot{q}_{HW,o}$ = hot-wall convective heat flux corrected for the effects of boundary-layer gas injection by means of the expression

$$\psi = \frac{\dot{q}_{HW}}{\dot{q}_{HW,o}} = \frac{aB}{[\exp(aB) - 1]} \qquad \text{(ref. 7)} \tag{3}$$

where $B = \dfrac{\dot{m}_w \Delta H_{BL}}{\dot{q}_{HW,o}}$

$\dot{q}_{rad}$ = absorbed gas-cap radiation heat flux

$\dot{q}_{comb}$ = heat liberated at the surface as a result of combustion of the char layer with the boundary-layer gases

$\dot{q}_{subl}$ = heat absorbed as a result of sublimation of carbon

$\dot{q}_{rr}$ = heat reradiated from the surface

$-K \frac{\partial T}{\partial x}$ = net heat conducted into the material

The effects on ψ of the mass-injection rate are shown in figure 8.

The continuity equation employed for the pyrolysis gases, as obtained from reference 3, is

$$\frac{\partial \rho}{\partial t} = \frac{\partial \dot{m}_g}{\partial x} = -A_1 (\rho - \rho_{char})^{\eta_1} \exp\left(\frac{-B_1}{T}\right) \tag{4}$$

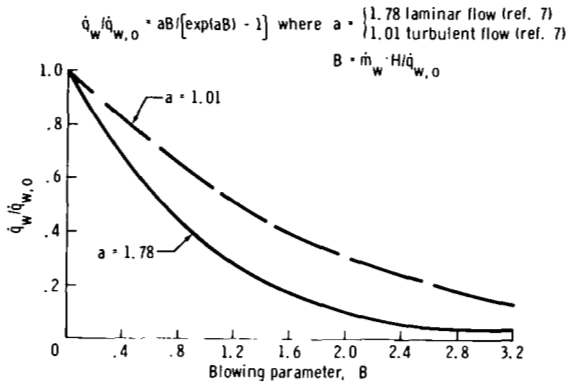

Figure 8.- Ratio of heat flux with blowing to heat flux without blowing as a function of the blowing parameter B and specie weighing factor a.

The char-deposition term of equation (1) was identified from ablator core analyses and has been included in the mass-balance equation of the STAB II computer program. Surface recession as a boundary condition can be easily applied by transforming equation (1) from a fixed coordinate system to a moving coordinate system whose origin moves with the char surface. The surface-recession-rate calculation based on the results of the ground test program discussed in reference 1 has been modified as a result of additional investigations and analyses of the flight test data. Both the char-deposition process and the surface-recession model are discussed in the section of this paper entitled "Ablation Model Uncertainties."

RESULTS AND COMPARISONS

Ablator Core Analysis

Laboratory studies.- Accurate material thermophysical property values are required for use in the ablation analysis if meaningful predictions of heat-shield thermal response are to be made. A study, described in reference 4, was initiated to provide limited measurements of the thermophysical properties of the Apollo ablation material from cores taken from a thermal-vacuum test article (spacecraft 008) and from the flown spacecraft of the Apollo 1, 3, and 4 missions. In addition, several selected ground test specimens, a virgin ablator test slab, and laboratory-charred test specimens were analyzed. During this study, measurements were made of apparent thermal conductivity (on the charred and virgin ablator test specimens) and of specific heat, and profiles of density and chemical composition were obtained. A detailed discussion of the experimental techniques used in measurement of the thermophysical properties is given in reference 4.

Figure 9 presents the results of an apparent (or effective) thermal conductivity test performed at three temperature levels on an ablator core taken from the Apollo 4 spacecraft. Figure 10, taken from reference 4, is a plot of apparent thermal conductivity as a function of the temperatures at which the material was charred in the laboratory. Figure 11 shows a comparison of the thermal conductivity data obtained from a typical postflight ablator core with the data determined from a laboratory-charred test specimen.

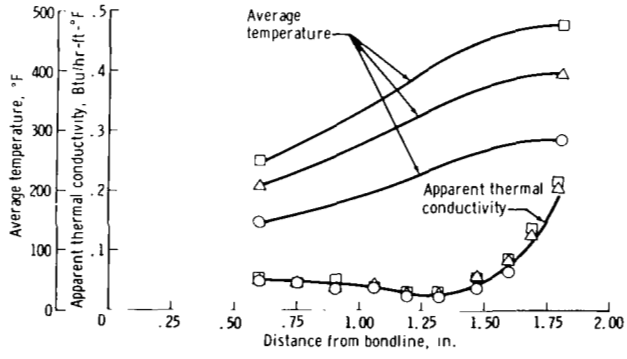

Figure 9.- Apparent thermal conductivity measurements obtained from a typical postflight ablator core.

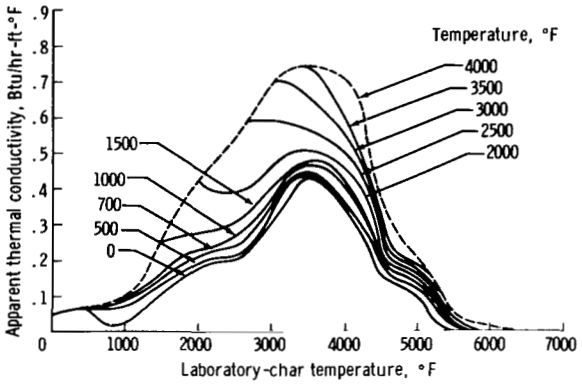

Figure 10. - Apparent thermal conductivity of the Apollo ablation material as a function of laboratory-char temperature.

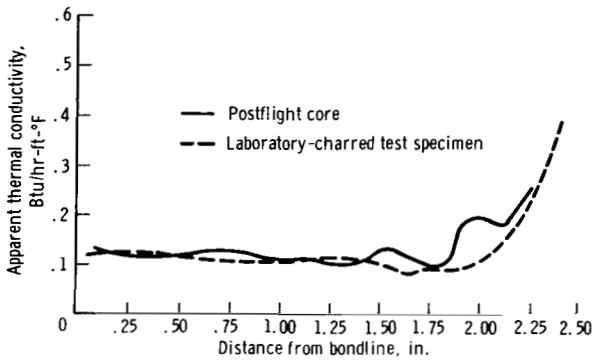

Figure 11. - Comparison of apparent thermal conductivity obtained from a typical postflight ablator core with apparent thermal conductivity determined from a laboratory-charred test specimen.

Measurements made of the ablator core density and ablator core chemistry profiles provided new insight into the thermal performance of the ablator. As shown by the density profile of a typical core (fig. 12), the ablator cores definitely show the effect of a carbon-deposition process. A corresponding chemical profile (fig. 13) for the core in figure 12 shows increasing carbon content near the aft-heat-shield surface. The effect of this carbon-deposition (or coking) process on surface recession and associated surface-energy balance is significant and will be discussed in the section of this paper entitled "Ablation Model Uncertainties."

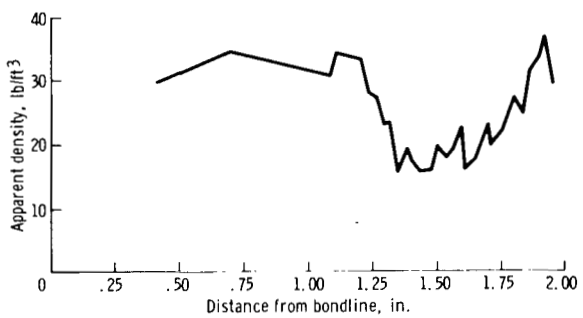

Figure 12. - Density profile of a typical postflight ablator core, showing the occurrence of the carbon-deposition process.

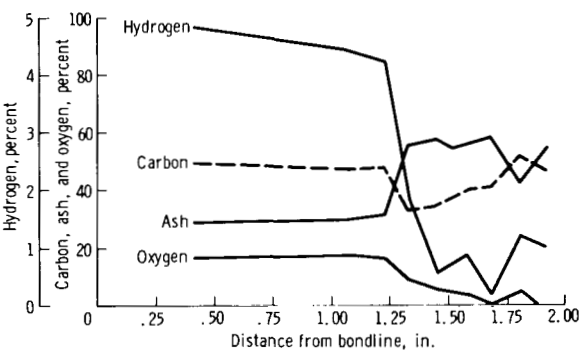

Figure 13. - Chemical profile of the same typical postflight ablator core shown in figure 12, showing increasing carbon content near the aft-heat-shield surface.

Analytical verification. - The transient response of a charring material is intimately coupled with the chemically reacting boundary-layer environment. Therefore, a decoupling of the boundary-layer/ablator-surface phenomenon from the indepth response was employed to verify the thermophysical property values used in the ablation analysis. However, this method of analysis is dependent upon the mathematical model used to simulate the indepth response of the material.

The indepth-temperature histories obtained from the Apollo 4 and 6 missions were used in the verification of the thermophysical properties of the heat shield. The temperature history of a near-surface thermocouple was used as the input boundary condition in the analysis in order to predict the temperature histories at deeper thermocouple locations. The results of using this "thermocouple driver" technique in predicting temperatures for a body point located on the 90° meridian (at $S/R_c = 0.97$) of the Apollo 4 and 6 heat shields are presented in figure 14. As shown, excellent agreement was obtained by using the properties presented in figure 10 and table II. Results obtained for other representative locations around the Apollo 4 spacecraft are presented in figure 15. The results show consistently good agreement, thus verifying the accuracy of the thermophysical property values obtained from laboratory-charred test specimens.

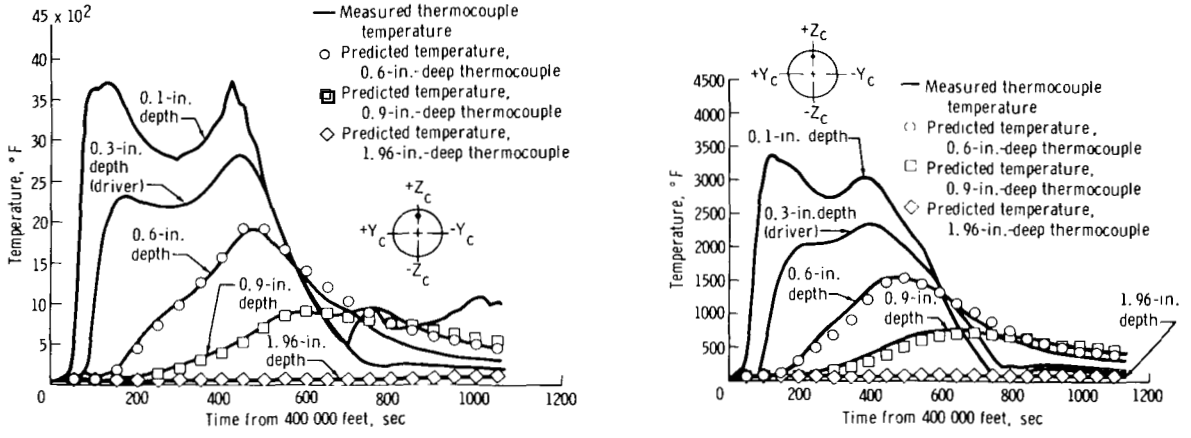

(a) Apollo 4: $Y_c = 0$ inch; $Z_c = 71.8$ inches.

(b) Apollo 6: $Y_c = 0$ inch; $Z_c = 71.8$ inches.

Figure 14. - Comparisons of measured temperatures with postflight-predicted temperatures calculated by using the near-surface thermocouple measurements as the input boundary condition; thermocouple depths are measured from the original ablator surface.

TABLE II. - SUMMARY OF MATERIAL PROPERTIES

(a) Constant property values

Specific heat of pyrolysis gas, $Btu/lb_m-°R$	0.5
Temperature at which surface recession begins, °R	2235
Density of virgin ablation material, lb_m/ft^3	32
Density of pure-char ablation material, lb_m/ft^3	20
Surface density, lb_m/ft^3	16
Emissivity of virgin ablation material[a]:	
Apollo 3 (all locations)	0.90
Apollo 4	
Aft heat shield	0.90
Leeward meridian, conical heat shield	0.40
Windward meridian, conical heat shield	0.90
Apollo 6 (all locations)	0.90
Emissivity of charred ablation material	0.65
Heat of combustion of carbon, Btu/lb_m	5000
Heat of degradation of virgin ablation material, $Btu/lb_m-°R$	180
Arrhenius coefficients:	
Reaction order, η_1	1.0
Specific reaction rate, A_1, hr^{-1}	9.5×10^8
Activation temperature, B_1, °R	2.33×10^5

[a]Virgin emissivity variation due to the thermal-control coating on the spacecraft.

TABLE II. - SUMMARY OF MATERIAL PROPERTIES - Concluded

(b) Specific heat as a function of temperature

Temperature, °R	Specific heat, c_p, Btu/lb_m-°R
Virgin material	
0	0.353
560	.348
660	.350
760	.370
860	.380
960	.420
1 060	.440
9 000	.440
Char material	
460	0.370
1 460	.370
2 460	.412
4 960	.412
5 460	.460
10 000	.460

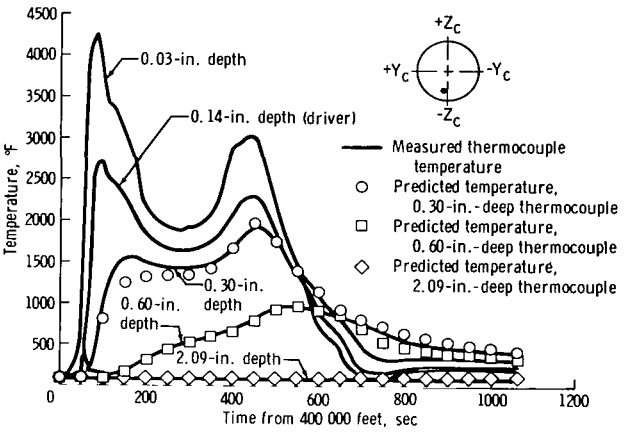

(a) Apollo 4: Y_c = 2.0 inches; Z_c = -50.0 inches.

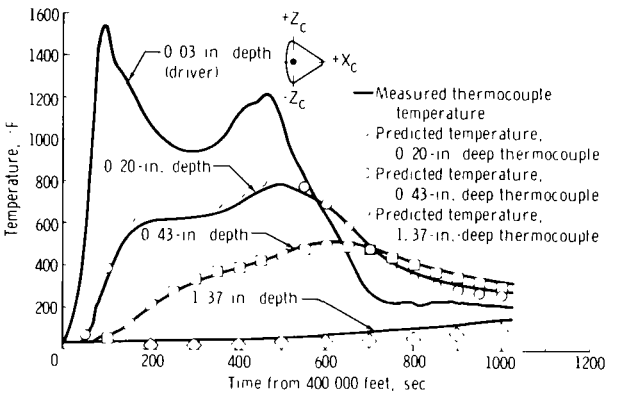

(b) Apollo 4: θ = 182°15'; X_c = 18.2 inches.

Figure 15. - Comparisons of Apollo 4 measured and postflight-predicted temperatures using the near-surface thermocouple measurements as the input boundary condition; thermocouple depths are measured from the original ablator surface.

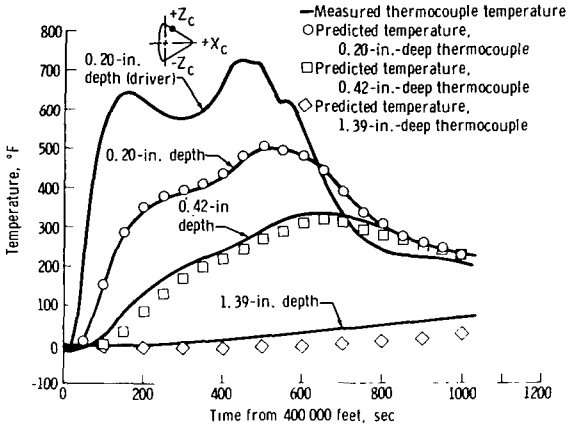

(c) Apollo 4: $\theta = 93°27'$; $X_c = 50.0$ inches.

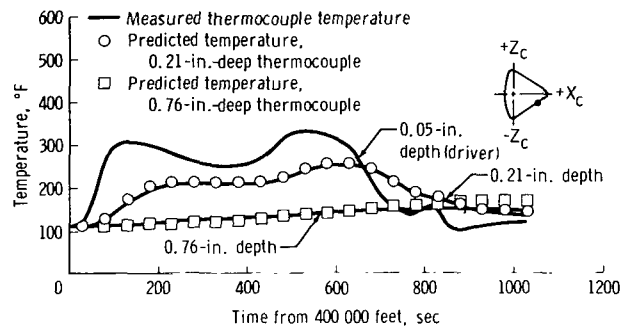

(d) Apollo 4: $\theta = 274°19'$; $X_c = 78.9$ inches.

Figure 15. - Concluded.

Comparisons of Measured and Postflight-Predicted Temperatures

The validity of the analytical model for prediction of ablative-heat-shield thermal response is demonstrated by comparing theoretical results with flight test data. Since the Apollo 4 and 6 heat shields had identical instrumentation, Apollo 6 heat-shield data were used to supplement the Apollo 4 data in the evaluation of heat-shield thermal performance at superorbital entry velocities. The postflight-predicted temperatures used in the evaluations are based on theoretically derived heating rates.

Aft heat shield. - Temperatures were measured by thermocouples located in depth at two smooth body locations on the aft heat shield of the Apollo 4 spacecraft. Figure 16(a) shows a comparison of measured and postflight-predicted temperatures obtained at a location on the pitch plane ($\theta = 90°$) near the area of maximum heating. To show the effect of different thermal environments on the same body location, results for Apollo 4 (fig. 16(a)) and 6 (fig. 16(b)) are presented. For Apollo 4, the postflight-predicted temperature of the ablator 0.1 inch from the surface exceeded the measured temperature during the first heating pulse, and surface recession was predicted to destroy the thermocouple at approximately 100 seconds. The predicted 0.22-inch surface loss compared favorably with the measured 0.19-inch surface loss at the thermocouple location. It should be noted that the thermocouple located 0.1 inch from the surface continued to show temperature response for the remainder of the entry. Based on laboratory test data, it is postulated that the thermocouple junction burned out and that as the wires receded with the ablator surface, the highly conductive charred ablation material formed a junction for the thermocouple wires and provided continuous temperature readings throughout the flight. The comparison between measured and postflight-predicted temperatures is considered excellent for all thermocouple depths, with perfect agreement being obtained at the bondline. The comparison of measured and postflight-predicted temperatures presented in figure 16(b) for the same body location on Apollo 6 shows comparable agreement.

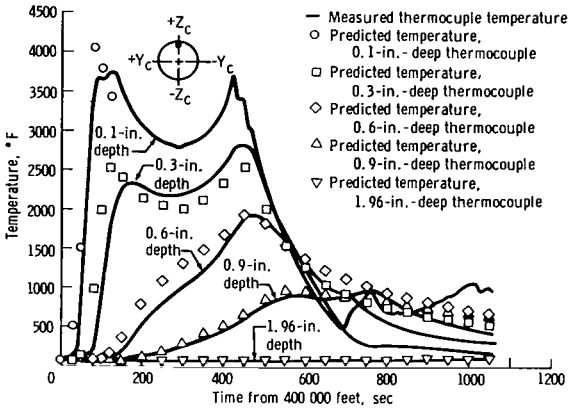

(a) Apollo 4: Y_c = 0 inch; Z_c = 71.8 inches.

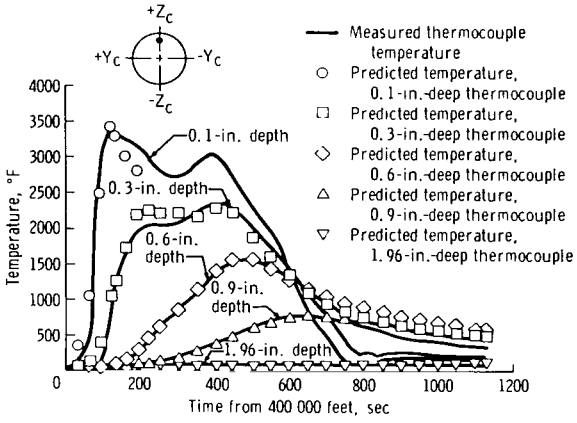

(b) Apollo 6: Y_c = 0 inch; Z_c = 71.8 inches.

The measured and postflight-predicted indepth temperatures at a location 50 inches downstream of the heat-shield center are shown in figure 16(c). During the first heating pulse, the predicted temperature closely approximated the measured temperature at a depth of 0.03 inch until the predicted surface recession exceeded that depth. The thermocouple, which was exposed as the surface receded, did not appear to be destroyed, but instead registered a temperature approaching 5200° F. After the thermocouple was exposed, it may have measured boundary-layer temperature rather than ablator-surface temperature. With the exception of the temperature at the bondline, where excellent agreement was obtained, the predicted temperatures were greater than the measured temperatures.

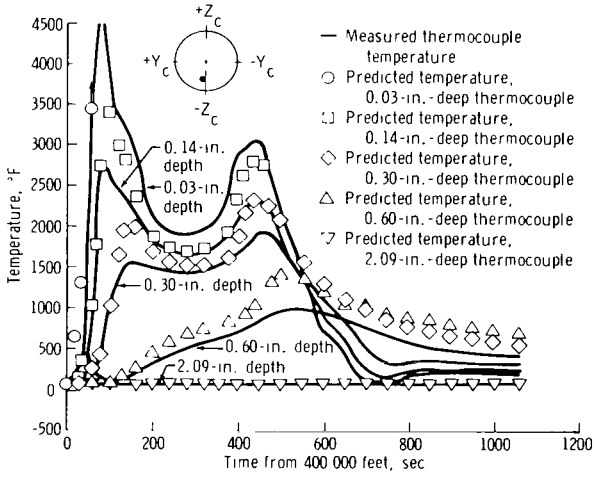

(c) Apollo 4: Y_c = 2.0 inches; Z_c = -50.0 inches.

Figure 16. - Comparisons of measured temperatures with postflight-predicted temperatures based on theoretical heating rates; thermocouple depths are measured from the original ablator surface.

Aft-heat-shield toroidal section. - The aft-heat-shield toroidal section is located between the aft heat shield and the conical heat shield. The maximum heat-shield diameter occurs within the toroidal section. For the Apollo 4 mission, indepth thermocouples were located near the maximum diameter at three positions around the circumference of the CM. Figure 16(d) shows a comparison of measured and postflight-predicted temperatures for a location on the toroidal section (θ = 182°15'). Predicted temperatures were higher than the temperatures measured by the

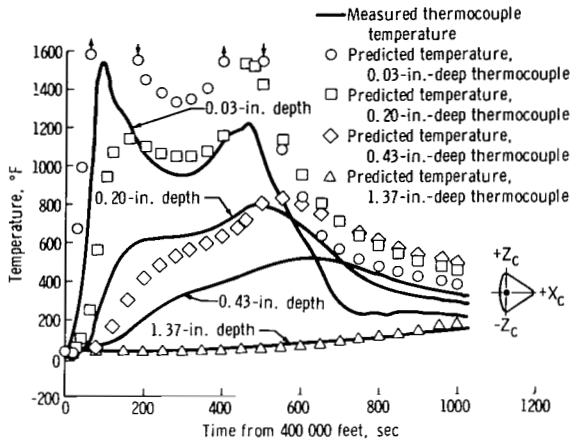

(d) Apollo 4: $\theta = 182^\circ 15'$; $X_c = 18.2$ inches.

Figure 16. - Continued.

thermocouples, with the exception of the predicted bondline temperature, which agreed closely with the measured bondline temperature.

The rapidly varying contour of the heat shield in the toroidal section and the accompanying changes in the aerodynamic flow field make assessment of the heating rate in the toroidal section difficult. The heating distribution curve in figure 3 shows a rapid change in the heating in the toroidal region. A small change in the body location, plotted as S/R_c, can result in a large change in the temperatures calculated when the heating distribution presented in figure 3 is used. However, the correlation shown for measured and predicted temperatures is considered acceptable for evaluating the performance of the aft-heat-shield toroidal section.

Conical heat shield. - Figures 16(e) and 16(f) present a comparison of measured and postflight-predicted temperatures for two typical body locations on the conical heat shield. Figure 16(e) shows results obtained at $X_c = 50$ inches on the windward meridian ($+Z_c$), and figure 16(f) shows the temperatures at $X_c = 78.9$ inches on the leeward meridian ($-Z_c$). Predicted temperatures on the windward meridian (fig. 16(e)) were consistently higher than measured temperatures at all depths, except at the bondline,

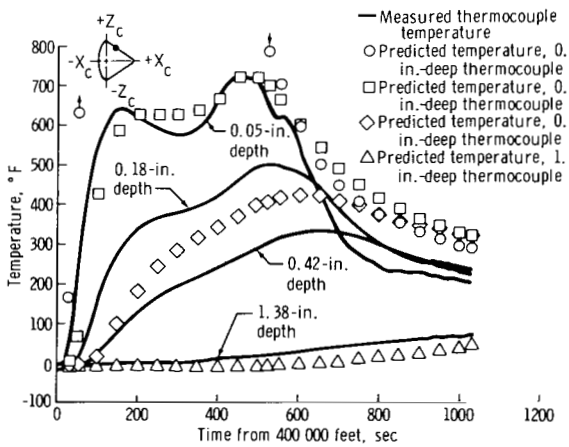

(e) Apollo 4: $\theta = 93^\circ 27'$; $X_c = 50.0$ inches.

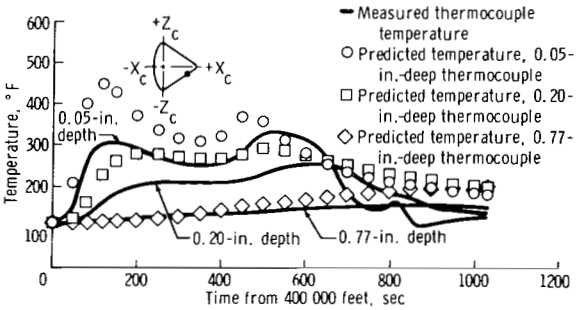

(f) Apollo 4: $\theta = 274^\circ 19'$; $X_c = 78.9$ inches.

Figure 16. - Concluded.

where the measured temperature was slightly greater than the predicted temperature. On the leeward meridian of the conical heat shield, the predicted temperatures were greater than the measured temperatures (fig. 16(f)).

Since it has been shown in figures 14 and 15 that good agreement between measured and postflight-predicted temperatures was obtained when the measured temperature response of the thermocouple nearest the surface was used as an input boundary condition, the overprediction of indepth temperatures shown in figures 16(c) to 16(f) is attributed to uncertainties in the calculated heating-environment data.

Comparisons of Measured and Postflight-Predicted Surface Recession and Char Penetration

Figure 17 presents a correlation of measured and postflight-predicted data for cores taken on the pitch plane (θ = 90° and θ = 270°). Figure 17(a) shows a comparison of measured and predicted ablator thicknesses. The surface recession (measured or predicted) can be calculated by subtracting the postflight results (measured or predicted) from the original ablator thickness profile. Figure 17(b) presents a comparison of measured and predicted char-penetration depths. The char penetration is the sum of the char thickness and the surface loss. This char interface indicates the 1000° F isotherm penetration and corresponds to a 95-percent decomposition of the virgin ablator material.

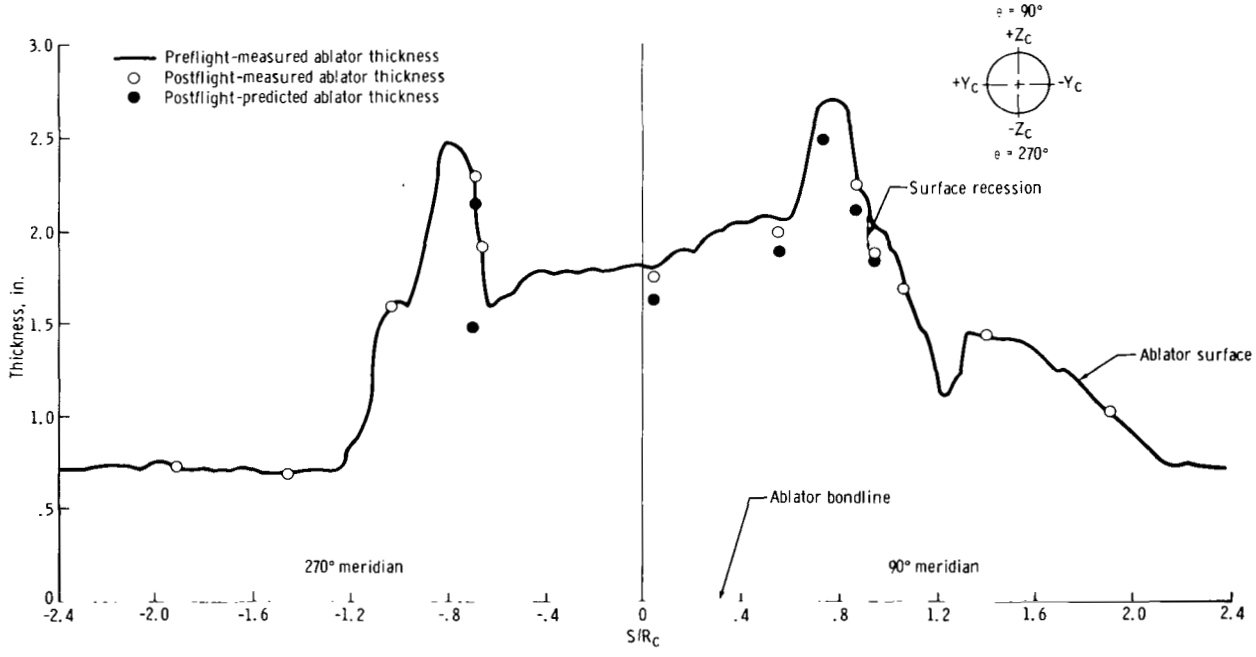

(a) Surface recession.

Figure 17. - Comparisons of measured and postflight-predicted ablator thermal performance based on cores removed from the Apollo 4 CM heat shield.

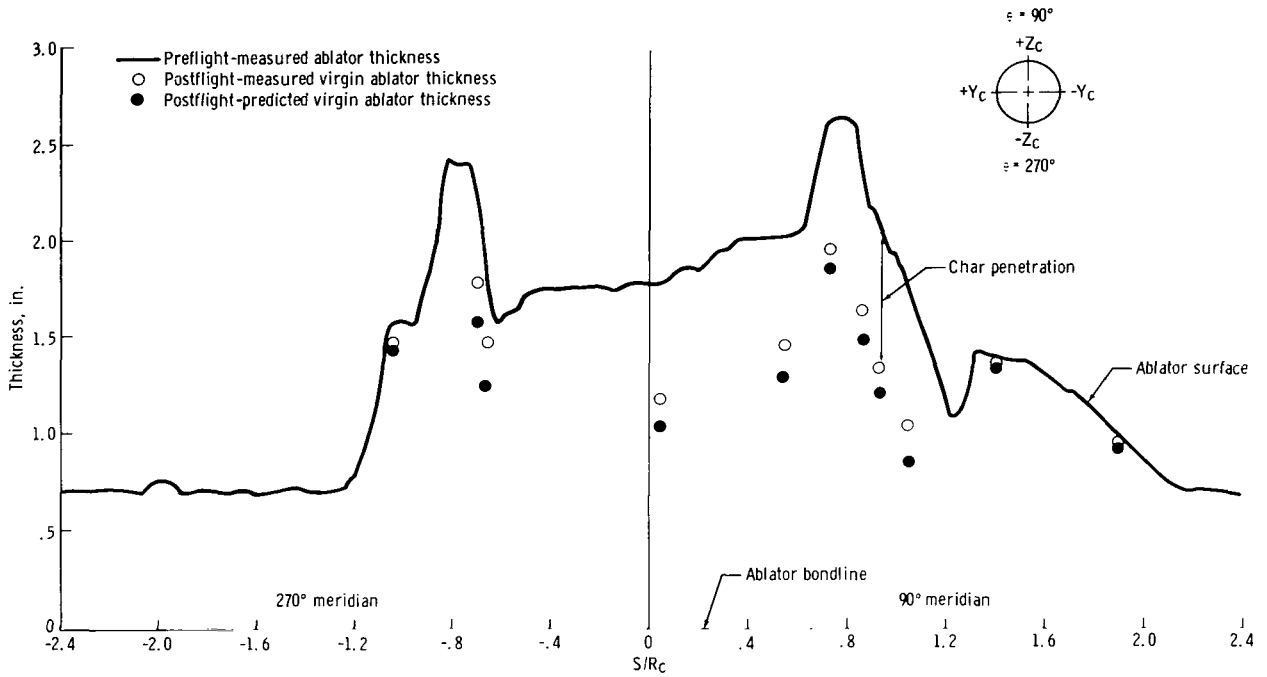

(b) Char penetration.

Figure 17. - Concluded.

Aft heat shield. - Both the surface-recession and the char-penetration values measured on the heat-shield cores show good agreement with postflight-predicted values.

Aft-heat-shield toroidal section and conical heat shield. - The effect of the changing heating environment around the aft-heat-shield toroidal section was clearly evidenced in the ablator cores taken from this region. Wide variation in the surface loss and char thickness occurred along the X_c-axis on each core. However, for comparable X_c locations, a consistent variation in ablator performance occurred around the circumference of the CM, with the greatest surface loss and char thickness occurring near the stagnation region ($\theta = 90^\circ$) and diminishing to negligible values at the leeward pitch plane ($\theta = 270^\circ$).

Negligible surface loss was measured from ablator cores taken from the conical heat shield. Char-thickness measurements averaged 0.05 inch on the windward meridian of the conical heat shield and diminished to no char on the leeward meridian of the conical heat shield.

ABLATION MODEL UNCERTAINTIES

Since no Apollo missions had been flown at the time the analytical model for the Apollo ablation material was developed, predictions of ablator thermal performance were checked against surface-recession, char-thickness, and indepth-temperature measurements obtained from an extensive ground test program performed in arc-heated facilities. As discussed in reference 1, good agreement was obtained between the predictions and the ground test results. However, the results of the flight tests demonstrated the need for additional studies and investigations to provide a better understanding of the ablation phenomenon. A discussion of the problem areas discovered during the flight tests is presented in the following paragraphs.

Surface Recession

Although the development of a theoretical surface-recession model and the experimental verification of surface recession for a graphite material were well known (ref. 8) at the time of the ground tests, a detailed theoretical surface-recession model for a composite ablation material had not yet been developed. However, the results of previous analytical and experimental studies (ref. 9) were used as a guide in developing a surface-recession model. The following approach was applied to the Apollo ablation material. The ground test data were analyzed to determine if the surface recession could be classified as an oxidation phenomenon in either the reaction-rate-controlled, the transition, or the diffusion-rate-controlled regime. The char mass-removal rate for the reaction-rate-controlled regime can be characterized by an equation of the Arrhenius form.

$$\dot{m}_{char} = \rho_{char}\dot{s} = K_o(P_o)^{\eta_2}\exp\left(-E/RT_S\right) \tag{5}$$

This equation suggests that the surface-recession test data could be correlated as a function of the reciprocal of surface temperature.

The char mass-removal rate for a diffusion-controlled oxidation process is given by an equation of the form

$$\dot{m}_{char} = C\left(\frac{\dot{q}}{\Delta H}\right) \tag{6}$$

Equation (6) suggests that the surface-recession rate is a function of the convective-heating rate and boundary-layer enthalpy potential. Better correlation of surface-recession data was obtained when the data were plotted as a function of $1/T_S$ (ref. 1). Accordingly, all preflight calculations were made by using a char-recession/surface-temperature correlation.

The preflight-predicted surface loss near the stagnation area for the Apollo 4 mission, which was calculated by using the char-recession/surface-temperature correlation, was approximately two to three times the measured value. Additional calculations for other locations on the spacecraft also showed the preflight surface-recession predictions to be conservative.

Preflight Apollo 4 predictions made by the Entry Structures Branch of the NASA Langley Research Center using a carbon oxidation model were in excellent agreement with the postflight results. Accordingly, the analysis was modified for better prediction of the observed flight surface recession. The ablator surface-recession predictions presented in this paper were computed by using the minimum char-erosion rate calculated from kinetically controlled and diffusion-controlled oxidation, as shown in the following equation.

$$\dot{m}_{char} = \text{minimum} \begin{cases} \dot{m}_{diff} = \rho_e u_e S T = \frac{12}{16} C_{o,e} \frac{\dot{q}_{WB}}{\Delta H_{BL}} \\ \dot{m}_{kine} = \rho_w \dot{s}(T_W) \end{cases} \tag{7}$$

where $\dot{s}(T_W)$ is obtained from the faired curve of figure 18. This modified surface-recession-rate relationship adequately predicted the measured data, as previously discussed, but underpredicted the ground test results.

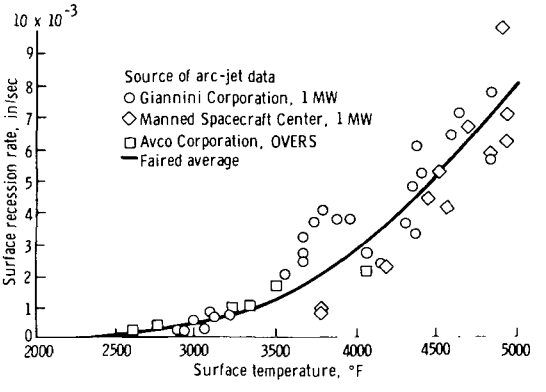

Figure 18. - Surface-recession correlation as a function of surface temperature.

An attempt to establish a better theoretical basis for the surface recession was made by using an equilibrium surface-chemistry program. This study is discussed in reference 10. Results of this investigation indicated that it was necessary to postulate (1) a mechanical removal of silica and (2) a mechanism that prevents oxygen depletion in the boundary layer by the pyrolysis-gas injection. With these postulated mechanisms, this model is capable of showing good correlation with both ground test data and flight test data. However, as discussed in reference 10, the postulated mechanisms are empirical and not completely satisfactory. Therefore, further development of such a model is considered necessary before a chemical-equilibrium approach to surface-recession analysis can be used for the Apollo ablation material.

Ablator-Density Effects

The results of postflight density and chemical analyses for Apollo 1, 3, and 4 heat-shield cores show that a carbon-deposition (or coking) process occurred in the char layer during the entry portion of each flight. Previous analyses for the Apollo ablation material (ref. 1) did not account for such a char-density increase. A simplified deposition model employing an Arrhenius-type equation has been postulated in the form

$$\dot{\rho}_{coke} = A_2(\rho_v - \rho)\exp(-B_2/T) \tag{8}$$

where the constants A_2 and B_2 are obtained from correlation with measured density profiles. Since the constants A_2 and B_2 were determined from the Apollo flight results and since the char-deposition rate described by equation (8) is independent of pyrolysis-gas mass flux, the use of equation (8) is applicable only to Apollo flight conditions. The char deposition is significant in the calculation of the surface-recession rate, convective-heat blocking (gaseous species and mass rate), and energy release or absorption by the char-deposition process. (The effect of the char-deposition process was accounted for in this paper in the surface-recession calculations for the diffusion-controlled regime.)

A comparison of the measured and postflight-predicted density profiles for a typical Apollo 4 ablator core is shown in figure 19; the results shown are typical of the agreement obtained with other postflight cores. As shown in equation (1), the deposition of carbon is considered in the analysis as an energy sink or source term. Since the results of a chemical-equilibrium calculation indicated the formation of a significant amount of methane (CH_4), it was assumed that the coking process could be described by the chemical reaction

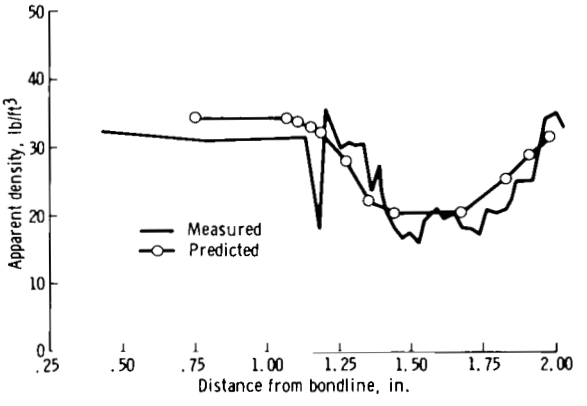

Figure 19. - Comparison of measured and postflight-predicted density profiles obtained from a typical Apollo 4 ablator core.

$$CH_{4(gas)} \longrightarrow C_{(solid)} + 2H_{2(gas)} \tag{9}$$

This reaction is an endothermic reaction with a heat of deposition (ref. 11) of 3220 Btu/lb_m (carbon) at 1800° R. Additional, as well as competing, chemical reactions can occur. However, the results obtained by using the approach employed in this analysis are encouraging. Equation (2) also indicates that an additional factor — the

composition of the injected gases — should be considered. The effect resulting from the molecular weight of the gases being injected into the boundary layer plays a dominant role in the convective-heat blocking effectiveness. Figure 20 (obtained from ref. 12) shows the relative blocking effectiveness on convective heating when inert carbon and inert hydrogen gases are injected into air. The convective-heat blocking curves (shown in fig. 8) used for the Apollo ablation material lie between the curves for inert carbon gas and inert hydrogen gas (fig. 20).

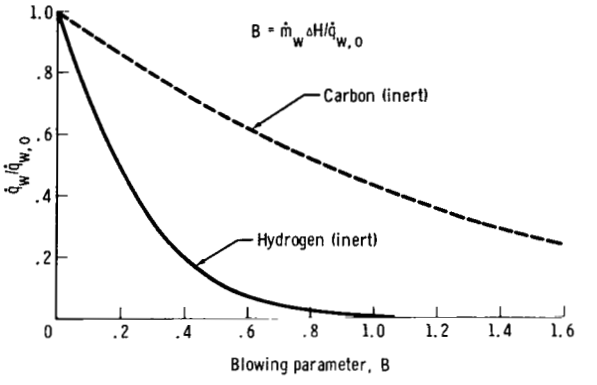

Figure 20. - Stagnation-point convective-heating blocking effectiveness for inert specie injection into air.

CONCLUDING REMARKS

Theoretical predictions of ablator thermal performance, obtained from an analytical model, have been used in conjunction with measured data to evaluate the thermal performance of the Apollo command module ablative heat shield at both earth-orbital and lunar-return entry speed conditions. The thermophysical property values used in the analytical model and obtained from laboratory-charred test specimens were shown to be consistent with thermophysical property values obtained from flight-tested ablator cores. Although analyses of flight test data indicate several uncertainties, such as the char-deposition process and the surface-recession mechanism, the adequacy of the analytical model to predict the thermal performance of the ablative heat shield of the Apollo command module for the expected range of flight environments has been demonstrated by the prediction of thermal performance for a lunar-return entry.

Manned Spacecraft Center
National Aeronautics and Space Administration
Houston, Texas, June 17, 1970
914-11-20-11-72

REFERENCES

1. Strouhal, G.; Curry, D. M.; and Janney, J. M.: Thermal Protection System Performance of the Apollo Command Module. Paper presented at the AIAA/ASME Seventh Structures and Materials Conference (Cocoa Beach, Fla.), Apr. 18-20, 1966.

2. Strouhal, George; Curry, Donald M.; and Posgay, Raymond G.: Definition of Entry Corridor Thermal Limits for Apollo Spacecraft. AIAA Paper No. 68-1144, AIAA Entry Vehicle Systems and Technology Meeting, Dec. 3-5, 1968.

3. Curry, Donald M.: An Analysis of a Charring Ablation Thermal Protection System. NASA TN D-3150, 1965.

4. Ihnat, Michael E.: Evaluation of the Thermophysical Properties of the Apollo Heat Shield, Vols. I and II. AVSSD-0375-67-RR (contract NAS 9-6940), AVCO Corporation, Aug. 8, 1967.

5. Bertin, John J.: The Effect of Protuberances, Cavities, and Angle of Attack on the Wind-Tunnel Pressure and Heat-Transfer Distribution for the Apollo Command Module. NASA TM X-1243, 1966.

6. Moen, Walter K.: Apollo Engineering Summary. Postrecovery Report - Heat Shield Instrumentation, CSM 101. TDR 68-166, Space Division, North American Rockwell Corporation, Dec. 1968.

7. Gomez, A. V.: Method of Evaluating Blowing Effects for the Apollo Heat Shield. Appendix H of Project Technical Report, Task E-45A. Third Summary Report, by H. H. Battley, R. G. Posgay, and I. Rubin. Rept. 05952-H420-R0-00 (contract NAS 9-4810), TRW Systems Group, Mar. 11, 1968.

8. Dow, Marvin B.; and Swann, Robert T.: Determination of Effects of Oxidation on Performance of Charring Ablators. NASA TR R-196, 1964.

9. Lundell, J. H.; Wakefield, R. M.; and Jones, G. W.: Experimental Investigation of a Charring Ablative Material Exposed to Combined Convective and Radiative Heating in Oxidizing and Nonoxidizing Environments. Paper presented at the AIAA Entry Technology Conference (Williamsburg and Hampton, Va.), Oct. 12-14, 1964.

10. Bartlett, Eugene P.; Anderson, Larry W.; and Curry, Donald M.: An Evaluation of Ablation Mechanisms for the Apollo Heat Shield Material. AIAA Paper No. 69-98, AIAA 7th Aerospace Sciences Meeting, Jan. 20-22, 1969.

11. McBride, Bonnie J.; Heimel, Sheldon; Ehlers, Janet G.; and Washington, Sanford G.: Thermodynamic Properties to 6000° K for 210 Substances Involving the First 18 Elements. NASA SP-3001, 1963.

12. Gomez, A. V.; and Mills, A. F.: Boundary Layer Heat and Mass Transfer Correlation Criteria for Apollo. Part II, Multicomponent Injection Correlation for Laminar Flow At The Stagnation Region Including Chemical Reactions. RN-68-3324. 2-4, TRW Systems, Inc., Aug. 5, 1968.

NASA-Langley, 1970 —— 33 S-247

"The aeronautical and space activities of the United States shall be conducted so as to contribute . . . to the expansion of human knowledge of phenomena in the atmosphere and space. The Administration shall provide for the widest practicable and appropriate dissemination of information concerning its activities and the results thereof."

—NATIONAL AERONAUTICS AND SPACE ACT OF 1958

NASA SCIENTIFIC AND TECHNICAL PUBLICATIONS

TECHNICAL REPORTS: Scientific and technical information considered important, complete, and a lasting contribution to existing knowledge.

TECHNICAL NOTES: Information less broad in scope but nevertheless of importance as a contribution to existing knowledge.

TECHNICAL MEMORANDUMS: Information receiving limited distribution because of preliminary data, security classification, or other reasons.

CONTRACTOR REPORTS: Scientific and technical information generated under a NASA contract or grant and considered an important contribution to existing knowledge.

TECHNICAL TRANSLATIONS: Information published in a foreign language considered to merit NASA distribution in English.

SPECIAL PUBLICATIONS: Information derived from or of value to NASA activities. Publications include conference proceedings, monographs, data compilations, handbooks, sourcebooks, and special bibliographies.

TECHNOLOGY UTILIZATION PUBLICATIONS: Information on technology used by NASA that may be of particular interest in commercial and other non-aerospace applications. Publications include Tech Briefs, Technology Utilization Reports and Notes, and Technology Surveys.

Details on the availability of these publications may be obtained from:

SCIENTIFIC AND TECHNICAL INFORMATION DIVISION

NATIONAL AERONAUTICS AND SPACE ADMINISTRATION

Washington, D.C. 20546